

Subwavelength Grating Devices in SOI

Junjia Wang¹, Reza Ashrafi¹, Ivan Glesk², and Lawrence R. Chen¹

¹Department of Electrical and Computer Engineering, McGill University, Montreal, QC H3A 0E9 Canada

²Department of Electronic and Electrical Engineering, University of Strathclyde, Glasgow, G1 1XU, UK

Abstract: We demonstrate subwavelength grating devices in silicon-on-insulator including Bragg gratings, racetrack resonators, and optical delay lines. The Bragg grating filter has a 3 dB bandwidth of 0.5 nm and a reflectivity of 90%; the racetrack resonator has a 3 dB bandwidth of 1 nm, a free spectral range of 4.6 nm, and an extinction ratio as high as 33 dB; the optical delay lines achieve ~30ps time-delay with 30% change in duty-cycle.

1. Introduction

There is an increasing need for integrated solutions in optical communications and interconnections applications [1]. In the past few years, a variety of active and passive devices as well as integrated subsystems in CMOS-compatible silicon photonics platforms have been realized [2]. Subwavelength grating (SWG) waveguides have attracted interest due to their potential for low loss and flexibility in tailoring the effective index [3,4]. Indeed, a number of SWG-based devices/building blocks in silicon-on-insulator (SOI) have been developed, including waveguide crossings [3], bends [4], couplers [4-6], and ring resonators [7]. Bragg gratings (BGs) and ring resonators have important applications as optical filters and for implementation in more complex wavelength selective devices. Optical delay line (ODL) devices are fundamental building blocks in all-optical and microwave photonic signal processing circuits. In this paper, we demonstrate SWG BG filters, race-track resonators, and ODLs.

2. SWG BGs

Fig. 1a compares the schematic of an SWG waveguide and an SWG BG in SOI. The effective index of the SWG waveguide depends on the duty cycle $f = a/\Lambda$, where a is the width of the high index medium (here Si) and Λ is the period. An SWG BG can then be realized by interleaving two SWG waveguides with different duty cycles $f_1 = a_1/\Lambda_1$ and $f_2 = a_2/\Lambda_2$; the SWG BG has a period of $\Lambda_1 + \Lambda_2$. By varying f_1 and f_2 , we create a periodic variation in the effective index and can thus obtain Bragg reflection. The cross-section of the SWG waveguides used in our experiments is shown in Fig. 1b. The width of the silicon layer is 500 nm and the thickness is 220 nm; it sits on top of a 3 μm thick buried oxide (BOX) layer and is covered by an index-matched 2 μm thick oxide cladding. We consider SWG waveguides with $\Lambda = 280$ nm to obtain a transmission window spanning the C-band and 1,000 periods. Two SWG tapers are used to

convert light into (and from) a Bloch mode before (and after) propagating through the SWG waveguide [5]. Vertical grating couplers (VGCs) [8] optimized for TE transmission are used to couple light in and out of the device. A compact Y-branch is used to extract the reflection response of the SWG BGs. The devices were fabricated using electron beam lithography with a single full etch. Figs. 1c and 1d show the SEM image of an SWG BG (before deposition of the top oxide cladding) and the full layout of the device.

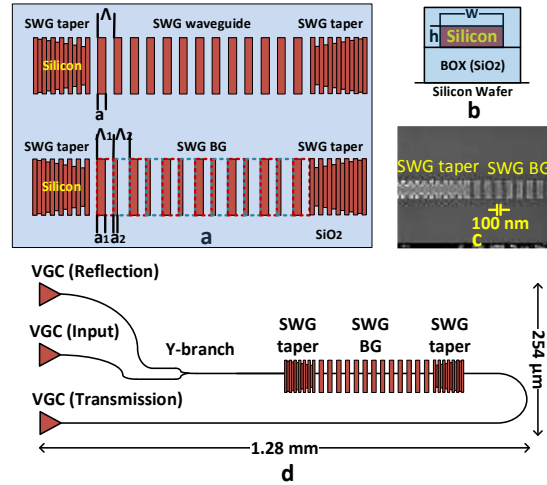


Fig. 1. (a) Top view of an SWG waveguide and an SWG BG, (b) device cross-section, (c) SEM of the fabricated SWG BG prior to top oxide cladding deposition, and (d) full layout.

Fig. 2a shows the measured transmission response of the SWG waveguide without and with an index modulation based on $f_1 = 50\%$ and $f_2 = 48\%$. There are no spectral features within the transmission window of the SWG waveguide; on the other hand, the SWG BG exhibits a clear rejection peak at a resonant wavelength of 1546.8 nm. Fig. 2b shows a zoom of the transmission and reflection responses around 1546.8 nm: the transmission loss is -12 dB corresponding to a peak reflectivity of 90.4%; the 3 dB bandwidth is 0.5 nm.

The total fiber-to-fiber loss is typically 15 dB (input port to reflection port).

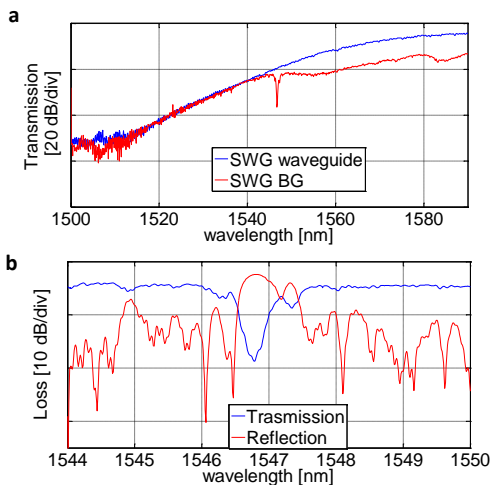


Fig. 2. Measured response of SWG waveguide and SWG BG ($f_1 = 50\%$ and $f_2 = 48\%$).

3. SWG Racetrack Resonators

In [5], we demonstrated SWG ring resonators that are under coupled. Racetrack resonators are preferable since the coupling region between the resonator and bus waveguides is longer compared to ring configurations, thereby allowing for greater control over coupling efficiency. Figs. 3a and 3b show the device layout and a zoom of the SWG racetrack resonator. The length of the directional coupling section is L and the separation between the bus and racetrack waveguides (center-to-center) is denoted g ; these two parameters determine the coupling efficiency and operating condition (under coupled, critically coupled, over coupled) of the resonator. The curved section has a radius r and the total perimeter of the racetrack which determines the free spectral range (FSR) is $2\pi r + 2L$. We use the same waveguide cross-section and VGC designs as for the SWG BGs. The SWG period is 300 nm and the duty cycle is 50% (to obtain a transmission window in the C-band).

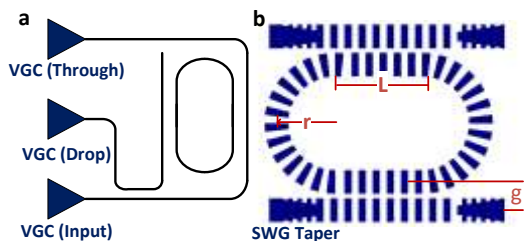


Fig. 3. Schematic of the (a) device layout, and (b) SWG racetrack resonator.

Fig. 4 shows the measured through and drop responses of an SWG racetrack resonator with $r =$

20 μm , $L = 40 \mu\text{m}$, and $g = 600 \text{ nm}$. The measured FSR is 4.6 nm, which agrees well with the value calculated using the total perimeter of the racetrack and effective waveguide index of 2.47. At 1527.9 nm, near critical coupling is achieved and we obtain an extinction ratio (ER) as high as 33 dB; the 3 dB bandwidth is 1 nm. The amplitude and ER variations are due to the wavelength dependence of the directional coupling.

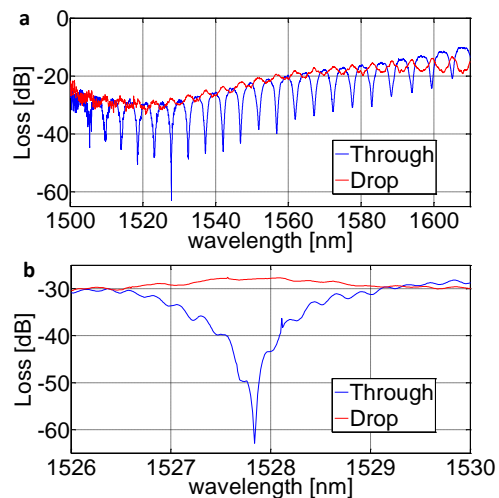


Fig. 4. (a) Measured through and drop responses of a SWG racetrack resonator with $r = 20 \mu\text{m}$, $L = 40 \mu\text{m}$, and $g = 600 \text{ nm}$. (b) Zoom in at one resonance at 1527.85 nm.

4. SWG Delay Lines

By choosing the duty cycle f , the effective (and group) index of the SWG waveguide can be modified and hence, optical delay can be realized. Fig. 5a shows a schematic of our proof-of-principle demonstration, which is a 4-tap ODL device on silicon-on-insulator (SOI) platform. The effective refractive index of the propagating Bloch mode in each tap of the fabricated ODL is a function of f . See [7] for a detailed numerical analysis about this. The corresponding generated time-delay difference between the taps of the ODL device can be expressed as

$$\Delta t(i) = [n_e(i+1) - n_e(i)] \cdot L/c, \quad 1 < i < N-1 \quad (1)$$

where c is the light speed in vacuum, and $N=4$ is the number of taps in the ODL. By properly designing the duty cycle f_i in each waveguide, the temporal separation between the taps can be controlled. Fig. 5b shows an SEM image of our fabricated device. The waveguide cross-section and VGC designs are the same as for the SWG BGs. The SWG period is 250 nm (to reduce losses and obtain a transmission window in the C-band). The designed duty cycles in SWG waveguides are $f_1=60\%$, $f_2=50\%$, $f_3=40\%$, and $f_4=30\%$. Six Y-branches (with 50:50 splitting ratio) were used to

split and collect the optical power at the input and output of the SWG waveguides, respectively.

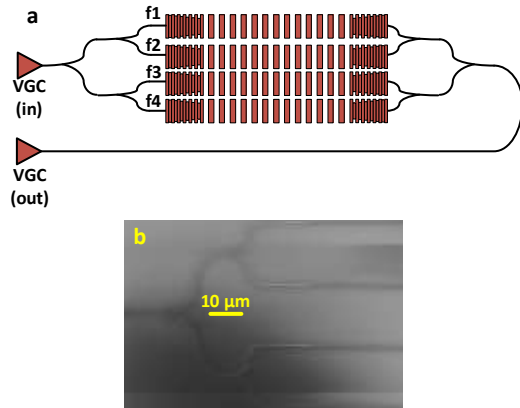


Fig. 5. (a) Schematic and (b) an SEM image of our fabricated 4-tap OD structure based on SWG waveguides in SOI.

Fig. 6 shows the measured spectral response of the fabricated OD device. At the input, we launch a Gaussian-like optical pulse with a full width at half maximum (FWHM) bandwidth of 2 nm at a central wavelength of 1556nm, which is generated using an actively mode-locked fiber laser with a repetition rate of 10GHz. Fig. 7 shows the generated time-domain output pulse train, measured using optical sampling oscilloscope. The signal spectrum at the input and output of the OD device is also shown in the inset of Fig. 7. As it can be seen in Fig. 7, the generated time-delay difference between the taps of the OD by introducing 10% change in duty cycles of SWG waveguides with 8mm length is ~ 9 ps. According to Eq. (1), this time-delay difference between the taps corresponds to an effective refractive index difference of 0.338 between the SWG waveguides. Note that as shown in Fig. 3, the pulse propagating through the SWG waveguide with lowest duty cycle (i.e. D_4) arrives faster than the other branches. The radiation loss increases as we decrease the duty cycle [9]. This can be seen in Fig. 7, where the output pulse corresponding to the waveguide branch with $f_4=30\%$ has the most amount of propagation loss. This additional loss can be compensated by properly designing the Y-branches with non 50:50 splitting ratios.

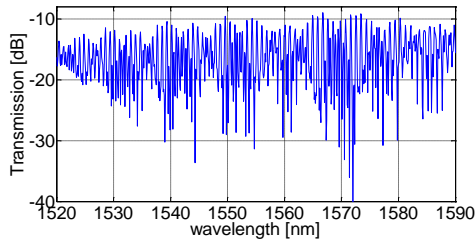


Fig. 6. Measured spectral response of the fabricated OD.

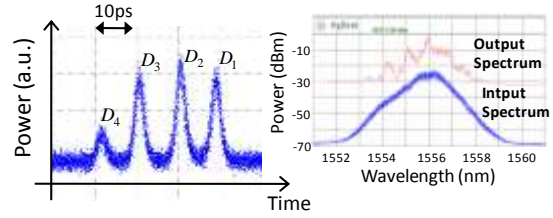


Fig. 7. Generated pulse train at the output of the fabricated OD device in response to a single input optical pulse. Input and output signal spectra have also shown in the inset.

5. Conclusions

We have demonstrated and experimentally verified SWG filters in SOI based on BGs and racetrack resonators. The SWG BG exhibits high reflectivity ($> 90\%$) and a relatively narrow reflection bandwidth (0.5 nm). The SWG racetrack resonator exhibits an extinction ratio as high as 33 dB. We also proposed a novel OD approach based on SWG waveguides in SOI. The obtained results clearly prove a great capability of the SWG waveguides to be employed in ODs to achieve a considerably compact structure. These devices are compatible with other SWG building blocks and can be used to develop more complex structures with enhanced functionality for applications in communications and sensing.

Acknowledgments

The devices were fabricated by R. Bojko at the University of Washington Nanofabrication Facility, a member of the NSF National Nanotechnology Infrastructure Network.

References

1. Y. Arakawa *et al*, *Ieee Commun Mag* **51**, 72-77 (2013).
2. Y. A. Vlasov, *Ieee Commun Mag* **50**, S67-S72 (2012).
3. P. J. Bock *et al*, *Optics Express* **18**, 16146-16155 (2010).
4. V. Donzella *et al*, *Optics Express* **22**, 21037-21050 (2014).
5. R. Halir *et al*, *Opt. Express* **20**, 13470-13477 (2012).
6. A. Ortega-Monux *et al*, *Photonics Technology Letters, IEEE* **23**, 1406-1408 (2011).
7. J. Wang *et al*, *Optics Express* **22**, 15335-15345 (2014).
8. Y. Wang *et al*, *Optics Express* **22**, 20652-20662 (2014).
9. D. Ortega *et al*, *J Lightwave Technol* **17**, 369-375 (1999).